Developmental Cell
Article

Integrin-Linked Kinase Controls Microtubule Dynamics Required for Plasma Membrane Targeting of Caveolae

Sara A. Wickström,[1,7,*] Anika Lange,[1] Michael W. Hess,[2] Julien Polleux,[1,3] Joachim P. Spatz,[3] Marcus Krüger,[4] Kristian Pfaller,[2] Armin Lambacher,[1] Wilhelm Bloch,[5] Matthias Mann,[4] Lukas A. Huber,[6] and Reinhard Fässler[1]
[1]Department of Molecular Medicine, Max-Planck Institute of Biochemistry, Am Klopferspitz 18, 82152 Martinsried, Germany
[2]Division of Histology and Embryology, Innsbruck Medical University, Müllerstrasse 59, 6020 Innsbruck, Austria
[3]Department of New Materials and Biosystems, Max Planck Institute for Metals Research, 70569 Stuttgart, Germany
[4]Department of Proteomics and Signal Transduction, Max-Planck Institute of Biochemistry, Am Klopferspitz 18, 82152 Martinsried, Germany
[5]Department of Molecular and Cellular Sport Medicine, 50933 Cologne, Germany
[6]Biocenter, Division of Cell Biology, Innsbruck Medical University, Fritz-Pregl Strasse 3, 6020 Innsbruck, Austria
[7]Present address: Max Planck Instutute for Biology of Ageing, Gleueler Strasse 50a, D-50931 Cologne, Germany
*Correspondence: wickstroem@age.mpg.de
DOI 10.1016/j.devcel.2010.09.007
Open access under CC BY-NC-ND license.

SUMMARY

Caveolae are specialized compartments of the plasma membrane that are involved in signaling, endocytosis, and cholesterol transport. Their formation requires the transport of caveolin-1 to the plasma membrane, but the molecular mechanisms regulating the transport are largely unknown. Here, we identify a critical role for adhesion-mediated signaling through β1 integrins and integrin-linked kinase (ILK) in caveolae formation. Mice lacking β1 integrins or ILK in keratinocytes have dramatically reduced numbers of plasma membrane caveolae in vivo, which is due to impaired transport of caveolin-1-containing vesicles along microtubules (MT) to the plasma membrane. Mechanistically, ILK promotes the recruitment of the F-actin binding protein IQGAP1 to the cell cortex, which, in turn, cooperates with its effector mDia1 to locally stabilize MTs and to allow stable insertion of caveolae into the plasma membrane. Our results assign an important role to the integrin/ILK complex for caveolar trafficking to the cell surface.

INTRODUCTION

Caveolae represent a specialized subclass of plasma membrane lipid domains present in several mammalian cell types. They play fundamental roles in the compartmentalization and organization of signaling pathways regulating cell growth and differentiation (Parton and Simons, 2007). The expression of caveolin-1, a transmembrane protein and main structural component of caveolae, is required for their formation, as mice lacking caveolin-1 also lack caveolae in all nonmuscle tissues (Drab et al., 2001). Caveolin-1 is synthesized in the endoplasmic reticulum, from where it enters the Golgi complex and caveolae assembly is believed to start. During its exit from the Golgi, caveolin binds cholesterol and forms detergent-insoluble oligomers (Pol et al., 2005), which are transported to the plasma membrane. Although these vesicles, termed caveolar carriers, appear to be distinct from other exocytotic vesicles, their exact molecular composition is still unknown (Parton et al., 2006; Tagawa et al., 2005). Exocytotic carriers in general move on microtubule (MT) tracks from the Golgi to the plasma membrane (Lippincott-Schwartz, 1998; Toomre et al., 1999), but whether this is also true for caveolar carriers remains to be shown. Once at the plasma membrane, caveolae are rather stable and become internalized upon specific stimuli, such as during viral entry or loss of cell adhesion (Pelkmans et al., 2002; Pelkmans and Zerial, 2005; del Pozo et al., 2005). Internalization of caveolae depends on the cortical F-actin network, which also constrains caveolae at the plasma membrane (Mundy et al., 2002; Pelkmans et al., 2002). Upon internalization, caveolae move along MT tracks and fuse with early and recycling endosomes, from where they can be recycled back to the plasma membrane (Mundy et al., 2002; Pelkmans et al., 2004; Tagawa et al., 2005).

We made the serendipitous observation that caveolar invaginations are absent from the plasma membrane of keratinocytes of mice lacking the expression of β1 integrin, or its key binding partner, integrin-linked kinase (ILK). Integrins are heterodimeric cell surface receptors that enable cell adhesion to extracellular matrix proteins. Upon ligand binding, integrins cluster and recruit adaptor and signaling proteins to their cytoplasmic domains, resulting in formation of small, immature adhesion sites called focal complexes (FCs) that eventually mature into large signaling hubs called focal adhesions (FAs) (Legate et al., 2009). An important integrin-binding protein is ILK, which can bind β1 integrin tails and regulate actin reorganization downstream of integrins (Wickström et al., 2010). Deletion of ILK in mice results in early embryonic lethality due to defects in epiblast polarity (Sakai et al., 2003). Mice with a targeted deletion of ILK in skin suffer from epidermal defects characterized by impaired polarity, attachment and migration of keratinocytes (Lorenz et al., 2007; Nakrieko et al., 2008).

We chose to investigate why keratinocytes lacking β1 integrin or ILK fail to develop normal numbers of caveolae. We found that ILK regulates the local stabilization of MTs, which, in turn, is

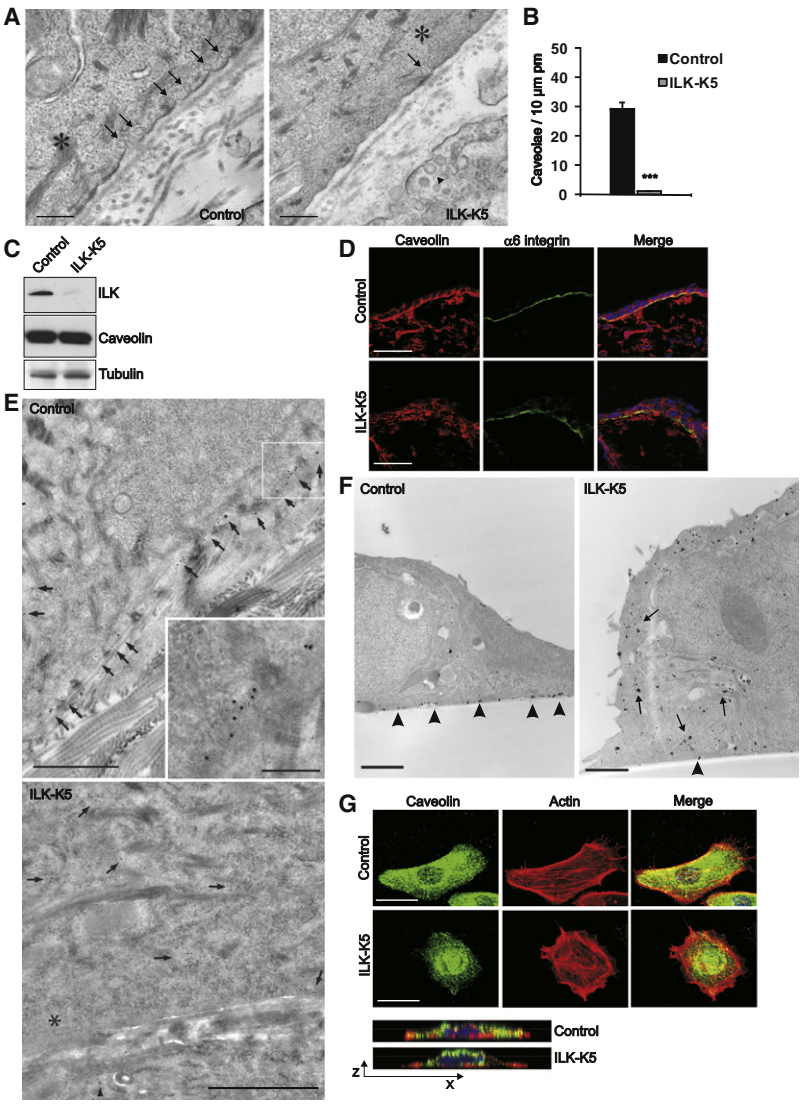

Figure 1. ILK Is Essential for the Formation of Plasma Membrane Caveolae

(A) EM shows multiple caveolae (arrows) at the basal plasma membrane of keratinocytes (asterisk) in control skin, while caveolae are almost absent in keratinocytes of ILK-K5 skin. Arrowheads mark caveolae in dermis of ILK-K5 skin, where ILK is not deleted. Scale bars, 250 nm.

(B) Quantification of plasma membrane (pm) caveolae (mean ± SEM; n = 3; ***$p < 0.0001$).

(C) ILK and caveolin-1 in keratinocyte lysates.

(D) Skin sections of control and ILK-K5 mice stained for caveolin-1 and α6 integrin. Scale bars, 25 μm.

(E) Cryosection immuno-EM of caveolin-1 in skin. Arrows mark 10 nm gold particles in basal keratinocytes (asterisk). Arrowheads mark gold particles within a dermal fibroblast. Scale bars, 1 μm. Insert shows higher magnification of caveolae in the framed area. Scale bar, 250 nm.

(F) Pre-embedding immuno-EM of caveolin-1 from primary keratinocytes. Arrowheads and arrows mark caveolin-1 at the plasma membrane and in the cytoplasm, respectively. Scale bars, 1 μm.

(G) Keratinocytes stained for caveolin-1 and F-actin. Confocal images from merged stacks shown in x-y (upper panels) and x-z (lowest panels) dimensions. Scale bars, 20 μm.

See also Figure S1 and S2.

critical for proper trafficking of caveolin-1-containing vesicles. ILK controls this process by regulating MT stability through the recruitment of the scaffold protein IQGAP1 and its downstream effector mDia1 to nascent, cortical adhesion sites. In the absence of ILK, caveolae remain associated with dynamic MTs, fail to stably fuse with the plasma membrane, and subsequently accumulate in intracellular structures.

RESULTS

The β1 Integrin/ILK Signaling Complex Is Required for Caveolae Formation

To delete the *Ilk* gene specifically in keratinocytes we intercrossed floxed ILK mice with a keratin 5 (K5) promoter-driven *Cre* recombinase strain (ILK-K5 mice). As described previously, ILK-K5 epidermis exhibits defects in keratinocyte polarity, adhesion, and basement membrane (BM) integrity (Lorenz et al., 2007; data not shown). We also observed, by electron microscopy (EM), that the number of caveolae was dramatically reduced at the basal plasma membrane of ILK-K5 keratinocytes when compared with controls (Figures 1A and 1B).

As ILK functions downstream of β1 integrins, we assessed whether the effect of ILK on plasma membrane caveolae is integrin dependent. We deleted the *β1 integrin* gene in the epidermis of mice (β1-K5) (Brakebusch et al., 2000) and analyzed their skin. ILK was no longer enriched at the basal side of basal keratinocytes (see Figure S1A available online). Primary β1 null keratinocytes were unable to form FAs, and displayed a diffuse ILK distribution, while keratinocytes lacking ILK still localized β1 integrin to FAs (Figure S1B and S1C). Similar to ILK-K5 skin, EM analysis also revealed a significantly reduced number of caveolae in basal keratinocytes of β1-K5 skin (Figure S1D and S1E). These results indicate that formation of plasma membrane caveolae depends on the β1 integrin/ILK complex.

Loss of ILK Decreases Plasma Membrane Caveolin-1 in Keratinocytes

The caveolin-1 protein is essential for the formation of caveolae (Drab et al., 2001). Western blot analyses excluded changes in the expression levels of caveolin-1 in lysates from ILK-K5 epidermis (Figure 1C). Next, we compared the distribution of caveolin-1 in epidermal keratinocytes from control and ILK-K5 mice. Normal back skin contained one layer of polarized, basal keratinocytes and one layer of postmitotic, suprabasal keratinocytes. In normal skin, the expression of caveolin-1 was restricted to the basal cell layer, where it localized predominantly to the basolateral surface of keratinocytes facing the BM (Figure 1D). As reported previously, ILK-K5 epidermis consists of a basal

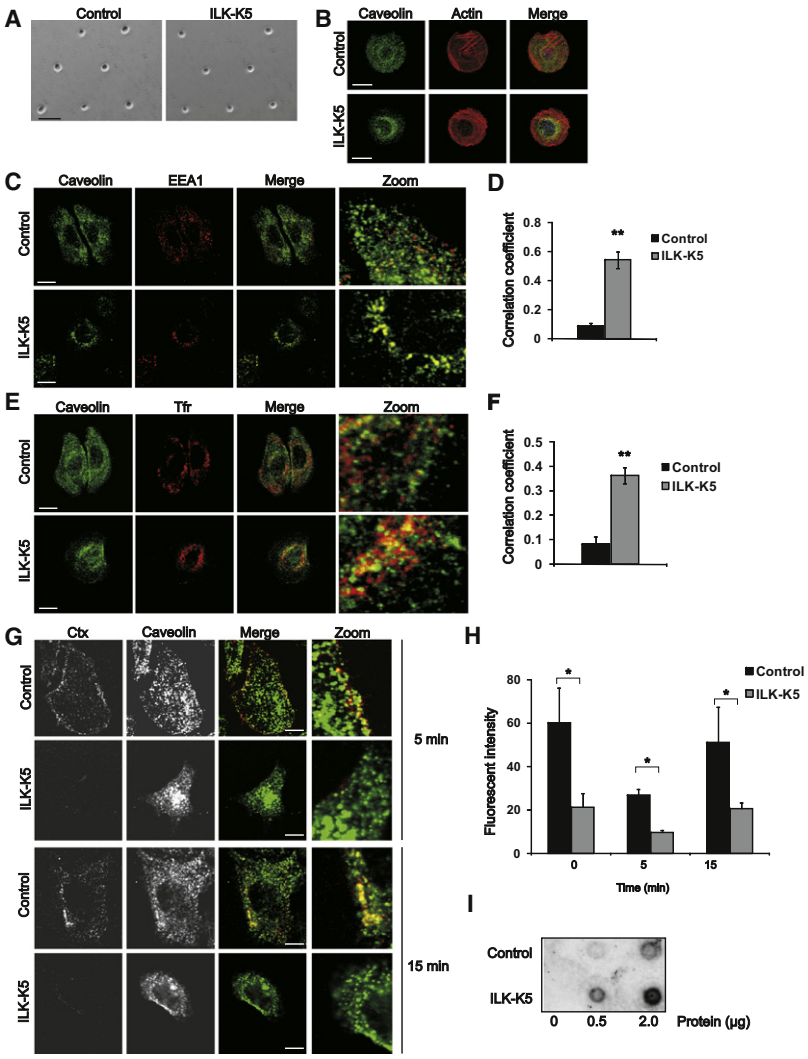

Figure 2. Altered Localization but Normal Internalization of Caveolin in ILK-K5 Cells

(A) Phase-contrast image of keratinocytes cultured on 20 μm-sized micropatterns. Scale bar, 60 μm.

(B) Keratinocytes on 20 μm-sized micropatterns stained for caveolin-1 and F-actin. Scale bars, 10 μm.

(C) Keratinocytes stained for caveolin-1 and early endosomal antigen 1 (EEA1). Scale bars, 15 μm.

(D) Quantification of colocalization of caveolin and EEA1 with Pearson's correlation coefficient (mean ± SEM; n = 6; **p = 0.0022).

(E) Keratinocytes stained with antibodies against caveolin-1 and transferrin receptor (Tfr). Scale bars, 15 μm.

(F) Quantification of colocalization of caveolin and Tfr (mean ± SEM; n = 5; **p = 0.0079).

(G) Keratinocytes were allowed to internalize fluorescent cholera toxin (Ctx), after which they were fixed and stained for caveolin-1. Scale bars, 15 μm.

(H) Keratinocytes were allowed to bind and internalize fluorescent Ctx and analyzed by flow cytometry (mean ± SEM; n = 5; *p = 0.0241).

(I) Keratinocyte lysates spotted on nitrocellulose were incubated with peroxidase-labeled Ctx.

See also Figure S2.

layer of keratinocytes, which lost their polar morphology and adopted a flattened shape, and multiple suprabasal layers of keratinocytes, which continue to express basal markers, such as K14, and β1 and β4 integrins (Lorenz et al., 2007). The expression of caveolin-1 was prominent in basal keratinocytes and also frequently observed in suprabasal cells of ILK-K5 epidermis (Figure 1D). Furthermore, the normal distribution of caveolin-1 was lost in basal ILK-K5 keratinocytes, and, instead, appeared throughout the cytoplasm (Figure 1D). The absence of caveolae, as well as the abnormal distribution of caveolin-1, was observed in areas with absent BM, as well as in areas with intact BM and hemidesmosomes, excluding the possibility that loss of BM integrity represents the trigger for the defective targeting of caveolin 1 (Figures 1A and 1D).

The abnormal distribution of caveolin-1 in ILK-K5 skin was confirmed by immuno-EM, which revealed dramatically reduced caveolin-1 staining at the basal plasma membrane and increased staining in the cytoplasm, while, in control skin, caveolin-1 staining was found almost exclusively associated with the basal plasma membrane (Figure 1E).

To confirm that the abnormal subcellular distribution of caveolin-1 in ILK-K5 keratinocytes is cell autonomous, we isolated primary keratinocytes from ILK-K5 mice and performed immuno-EM on these cells. These analyses confirmed the reduction of plasma membrane-associated caveolin-1 in ILK-K5 cells (Figure 1F). Semiquantitative estimation of immunogold labeling on keratinocyte cryosections showed that caveolin-1 labeling localized predominantly at and in close vicinity to the plasma membrane of control cells (~66% of total label peripheral, ~33% intracellular), whereas ILK-K5 cells showed an increased intracellular caveolin-1 labeling (~33% peripheral, ~66% intracellular). The altered distribution of caveolin-1 was further substantiated by immunofluorescence analyses where primary keratinocytes were stained for caveolin-1 and F-actin. In control keratinocytes caveolin-1 was targeted to the cell periphery, while, in ILK-K5 keratinocytes, caveolin-1 localized preferentially around the nucleus (Figure 1G; Figure S2A). The same was observed in β1 null keratinocytes (Figure S2B).

To exclude that the altered localization of caveolin-1 could be an indirect effect caused by reduced cell spreading and increased rounding of ILK-K5 keratinocytes, we used deep UV lithography to micropattern circular fibronectin-coated islands with a diameter of 20 μm (Azioune et al., 2009; Blummel et al., 2007). Cells adhering to the islands had a defined spreading area, and the cell shape and surface area of control and ILK-K5 cells were found to be comparable (Figure 2A). Immunofluorescence analysis of these cells revealed that caveolin was still targeted to the cell periphery in control cells, whereas perinuclear accumulation was observed in ILK-K5 cells (Figure 2B).

To determine the subcellular localization of caveolin-1 in ILK-K5 cells, we performed double staining of caveolin-1 with the

early endosomal antigen 1, a marker for early endosomes, as well as transferrin receptor, a marker for recycling endosomes, and found that the cytoplasmic caveolin in the ILK-K5 cells partially colocalized with both markers (Figures 2C–2F). No colocalization was observed with lysosomal markers (data not shown).

Loss of cell-matrix adhesion has been shown to result in rapid internalization of caveolar membrane domains, associated with the removal of Rac1 from the plasma membrane and downregulation of Akt and Erk activities (del Pozo et al., 2004, 2005). However, Akt and Erk phosphorylation (Lorenz et al., 2007), as well as the levels of membrane-associated Rac1 (Figure S2C), are all unchanged in ILK-K5 cells. Moreover, ligand internalization assays with fluorescent cholera toxin subunit B (Ctx), which binds the cell surface ganglioside GM1 and is internalized primarily through caveolae (Parton et al., 1994), revealed that binding of Ctx to the plasma membrane of ILK-K5 cells was significantly reduced, and that internalization of Ctx was decreased proportionally to the total cell surface levels (Figures 2G and 2H). The binding of Ctx to cell extracts was slightly increased in ILK-K5 cells (Figure 2I), excluding the possibility that the reduction in cell surface binding and internalization were due to a decrease in total GM1 levels. These experiments strongly indicate that the absence of plasma membrane caveolae in ILK-K5 cells is not due to increased internalization rates.

The formation of lipid domains upon caveolin-1 binding to cholesterol represents the initial step of caveolae formation, which most likely occurs shortly before or during the exit from the Golgi apparatus (Parton et al., 2006). This results in the partitioning of caveolin into detergent-resistant membranes (DRMs), which can be separated by density centrifugation. In lipid rafts isolated from ILK-K5 cells, caveolin-1 still floated with DRMs, indicating that the formation of caveolar lipid domains is normal, and that initial biogenesis of caveolae occurs independently of ILK (Figure S2D). In addition, we observed no obvious colocalization or interaction between ILK and caveolin-1, indicating that ILK regulates caveolin-1 through an indirect mechanism (Figures S2E–S2G).

ILK Controls Dynamics of Caveolae

To test whether the abnormal caveolin-1 distribution in ILK-K5 keratinocytes is a result of altered caveolar dynamics, we expressed EGFP-tagged caveolin-1 and performed live-cell imaging by total internal reflection fluorescence (TIRF) microscopy. In line with a previous study (Pelkmans and Zerial, 2005), the majority of EGFP-caveolin containing vesicles (87 ± 4%) in control cells remained stable for the duration of imaging. In contrast, the pool of stable caveolae was significantly reduced in ILK-K5 cells and 52 ± 5% of EGFP-caveolin vesicles displayed an extremely dynamic behavior, characterized by frequent appearing and disappearing of EGFP-caveolin-1 from the TIRF field (Figures 3A amd 3B; Movie S1). Stable plasma membrane caveolae could be restored by transient re-expression of ILK in ILK-K5 cells (Figures 3A and 3B). The total number of caveolin-1-positive vesicles in the TIRF field remained constant over time in both control and ILK-K5 cells (Figure 3C). The absence of a net loss of EGFP-caveolin in ILK-K5 cells over time indicates bidirectional motility of caveolin-1 vesicles. Importantly, reduced cell spreading did not influence caveolar dynamics, as control cells adhering on 20 μm-sized micropatterns retained the stationary phenotype of caveolar motility despite reduced spreading, whereas caveolae in ILK-K5 cells displayed increased motility irrespective of whether plated on micropatterns or not (Figure S3A).

As cortical actin has been shown to mediate the motility of caveolae close to the plasma membrane (Mundy et al., 2002; Pelkmans et al., 2002), we addressed whether the altered pattern of caveolar motility in ILK-K5 cells results from altered actin-based motility. To this end, we transfected keratinocytes with EGFP-caveolin-1 and the actin marker Lifeact (Riedl et al., 2008), and analyzed them by spinning-disc microscopy. These experiments revealed that a fraction of the peripheral, static caveolin-containing vesicles of control cells colocalized with cortical F-actin fibers, whereas no colocalization with actin was observed in ILK-K5 cells (Figures S3B and S3C). The experiments also showed that the increased caveolar dynamics in ILK-K5 cells were not an indirect effect of increased lamellipodial dynamics, as the lamella remained static over the duration of the imaging, whereas the caveolin-containing vesicles underwent extensive motility (Figures S3B and S3C).

Increased MT-Based Motility of Peripheral Caveolae in ILK-K5 Cells

Since caveolae recycle along MT tracks between the plasma membrane and endosomal compartments (Mundy et al., 2002; Tagawa et al., 2005), we imaged MT-based motility of caveolae by transfecting keratinocytes with EGFP-caveolin-1 and Cherry-tubulin. The experiments revealed that peripheral caveolae in control cells were static, and only a minor population underwent motility along MTs. In contrast, caveolae in ILK-K5 cells were highly dynamic and frequently trafficked on growing MTs to the periphery, and, upon MT shortening, moved back toward the cell center (Figure 3D; Movie S2). We quantified this change in motility by tracking individual caveolae. The tracks of motile caveolae had a high degree of correlation with the directionality vectors of their nearest MTs when compared with the correlation with mathematically modeled, random isotropic motility (Figure 3E), supporting the visual observation that caveolae in ILK-K5 cells move along MTs. In addition, peripheral caveolae in ILK-K5 cells moved with higher velocity and over longer distances compared with control cells (Figures 3F and 3G). In contrast, fluorescent recovery after photobleaching assays and individual tracking of caveolar carriers revealed that the velocity of central caveolae was similar in control and ILK-K5 cells (Figures S3D–S3F).

The dependence of caveolar motility on MTs was further confirmed by disrupting MTs with 1 μM nocadozole and subsequently analyzing EGFP-caveolin-1 motility by TIRF. Nocadozole treatment resulted in a marked decrease of caveolar vesicles visible in the TIRF field of ILK-K5 cells, while it had little effect on plasma membrane motility of caveolae in control cells (data not shown). As caveolae moved preferentially along dynamic MTs, we next determined whether the dynamic instability of MTs affects caveolar trafficking, as has been observed for other vesicular carriers previously (Lomakin et al., 2009). First, we treated ILK-K5 cells with a combination of low concentrations of nocodazole (50 nM) and taxol (1 μM) to inhibit MT growth and catastrophe without disrupting the MTs themselves (Buck and Zheng, 2002). Under these conditions, caveolae detached

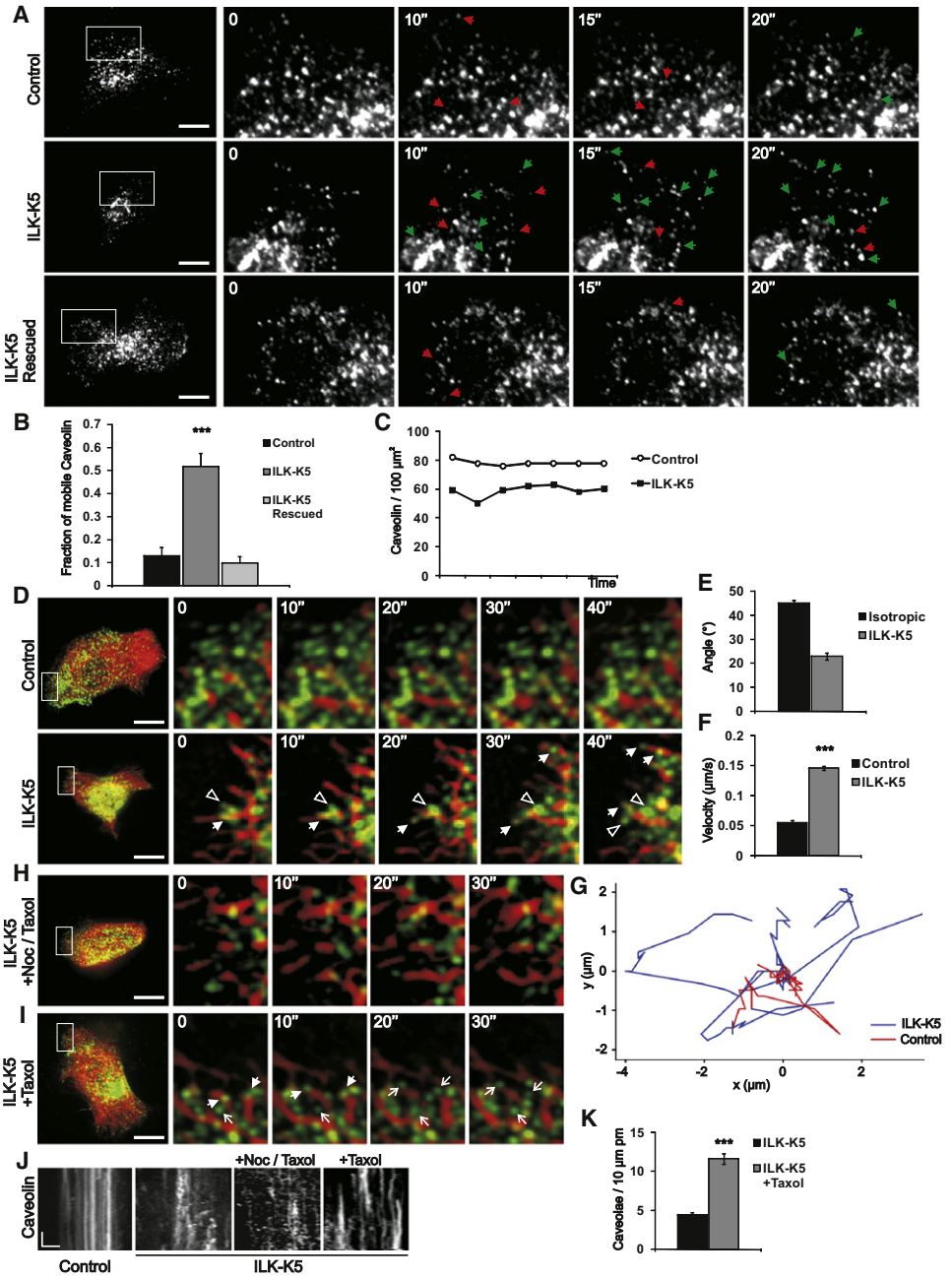

Figure 3. Altered Dynamics of Caveolin-1 in the Absence of ILK

(A) Dynamics of EGFP-caveolin-1 near the plasma membrane analyzed by TIRF in control, ILK-K5, and ILK-K5 cells reconstituted with ILK. Images are snapshots from Movie S1 acquired at ~200 ms/frame. Right panels show an enlargement of the area indicated by the white rectangle. Green and red arrowheads indicate appearing and disappearing vesicles, respectively. Scale bars, 10 µm.

(B) Quantification of mobile caveolin-1 (mean ± SEM; n = 8; ***p(ANOVA) F = 31.54; R^2 = 0.07328).

(C) Quantification of the total amount of EGFP-caveolin-1-positive vesicles in control and ILK-K5 cells as a function of time. A representative experiment is shown.

(D) Dynamics of caveolae (green) and MTs (red) analyzed by spinning-disc microscopy in control and ILK-K5 keratinocytes. Images are snapshots from Movie S2 acquired at 2 s/frame. Right panels show an enlargement of the area indicated by the white rectangle. Closed and open arrowheads indicate vesicles moving on MTs toward the periphery and inwards, respectively. Scale bars, 10 µm.

(E) Average angles of directionality vectors from tracked caveolae and MTs in ILK-K5 cells compared with calculated angle distribution of isotropic motility (mean ± SEM; n = 45 vesicles from 5 cells).

(F) Velocity of peripheral caveolae in control and ILK-K5 cells (mean ± SEM; n = 45 vesicles from 5 cells; ***p < 0.0001).

(G) Representative tracks of peripheral caveolae in control and ILK-K5 cells.

(H) Dynamics of caveolin-containing vesicles (green) and MTs (red) analyzed in ILK-K5 keratinocytes treated with 50 nM nocadozole and 1 µM taxol. Images are snapshots from Movie S3 acquired at 2 s/frame. Right panels show an enlargement of the area indicated by the white rectangle. Scale bar, 10 µm.

from the stable MTs and underwent rapid, random motility in the cytoplasm (Figure 3H; Movie S3), indicating that caveolae associate with dynamic MTs. Next, we treated cells with low concentrations of taxol (3 nM) to inhibit MT catastrophe, but still allowing MT growth (Buck and Zheng, 2002). Under these conditions, caveolae still moved along MTs to the cell periphery where they were subsequently stabilized. Furthermore, multiple stable caveolae were detected in the cell periphery (Figure 3I; Movie S3). Kymographs from the movies confirmed the enhanced motility of caveolae in ILK-K5 cells and restoration of stable caveolae upon taxol treatment (Figure 3J). To correlate the stabilization of peripheral caveolin-positive vesicles to the ability of the cells to form plasma membrane caveolae, we performed quantitative analyses of plasma membrane caveolae in untreated and taxol-treated ILK-K5 cells by EM (Figure 3K). These experiments suggest that both plus- and minus-ended traffic of caveolin-containing vesicles occur on dynamic MTs, and inhibition of MT catastrophe leads to the stabilization of peripheral caveolae.

ILK Regulates MT Distribution and Stability

The increased MT-based dynamics and concomitant decrease in actin-based motility of caveolae suggest that cytoskeletal defects might underlie the abnormal caveolar targeting in ILK-K5 cells. Therefore, we examined the MT and F-actin networks in more detail. In agreement with our previous report (Lorenz et al., 2007), ILK-K5 keratinocytes showed F-actin defects and reduced spreading (Figure 4A; Figure S1C). In addition, the MT network of ILK-K5 cells was abnormal, with compact and dense packs of MTs in the center and significantly decreased density in the periphery. Furthermore, peripheral MTs failed to reach the cell cortex (Figure 4A). The altered distribution of MTs was not due to the decreased spreading of ILK-K5 cells, as the same defect was observed on 20 μm-sized micropatterns (data not shown).

MT stabilization requires the interaction of MT plus-end-binding proteins with the cell cortex. In control cells, a large proportion of MTs stained positive for acetylated tubulin, a post-translational modification associated with stabilized MTs. Strikingly, only low levels of acetylated tubulin were detected in ILK-K5 cells (Figure 4B), which was confirmed by western blotting (Figures 4C and 4D). Treatment of cells with taxol, which increases the levels of acetylated tubulin by stabilizing MTs (Yvon et al., 1999), induced comparable levels of acetylated tubulin in control and ILK-K5 cells (Figure 4E), indicating that tubulin acetylation itself can be induced in the absence of ILK, and that ILK regulates tubulin acetylation indirectly by regulating MT stability. The reduction in MT stability of ILK-K5 cells was further confirmed by treating cells with nocodazole, which revealed a reduced MT resistance in the absence of ILK expression (Figure 4F). Live imaging of EGFP-tubulin-transfected cells revealed that the peripheral MTs in control keratinocytes were extremely stable, while the majority of MTs in ILK-K5 cells were dynamic, characterized by increased catastrophe frequency and decreased duration of pauses between phases of growth and shortening (Figure 4G; Table S1A and Movie S4).

MT Dynamics Regulate Trafficking of Caveolae

As we observed defects both in the actin and MT cytoskeletons, we sought to determine the potential contribution of these defects to the altered caveolar trafficking in ILK-K5 cells. The internalization of caveolae requires an intact and dynamic actin cytoskeleton, as inhibition of actin polymerization by latrunculin B (LatB) blocks this process (Pelkmans et al., 2002). On the other hand, cortical actin was shown to stabilize plasma membrane caveolae (Mundy et al., 2002). To determine whether the loss of stable plasma membrane caveolae was a result of altered actin polymerization, we treated EGFP-caveolin-1-transfected cells with LatB and analyzed caveolar dynamics by spinning-disc and TIRF microscopy. LatB treatment increased the peripheral density of caveolae in control cells, but not in ILK-K5 cells (Figures 5A and 5B). Furthermore, LatB treatment of ILK-K5 cells did not significantly stabilize peripheral caveolae, or increase the motility of caveolae in control cells (Figures 5A–5C), suggesting that aberrant actin polymerization was not causing increased caveolar dynamics in ILK-K5 cells.

To address whether increased caveolar dynamics was due to the observed increased catastrophe frequency of MTs, we transfected control cells with the C-terminal fragment of the plus-end-binding protein EB1 (EB1-CΔAC), which lacks the MT-binding domain. EB1-CΔAC acts as a dominant negative EB by forming heterodimers with wild-type EB proteins, reducing their affinity to MTs, thereby inhibiting their ability to protect MTs from catastrophe (Komarova et al., 2009). Expression of EB1-CΔAC led to increased MT dynamics (data not shown) and increased caveolar trafficking along MTs in the periphery of control keratinocytes (Figure 5D; Movie S5) resembling the behavior of caveolin in ILK-K5 cells (Figure 3D). The effect of EB1-CΔAC on caveolar motility was further confirmed by TIRF microscopy (Figures 5E and 5F; Movie S6). Collectively, these results demonstrate that MT dynamics regulate caveolar traffic, and that increased catastrophe frequency of MTs leads to the loss of stable plasma membrane caveolae.

ILK Binds and Regulates the Subcellular Distribution of IQGAP1

To test whether ILK is part of an MT capture complex that binds cortical F-actin and MT tips and links them together (Rodriguez et al., 2003), we screened for novel ILK interaction partners by utilizing stable isotope labeling by amino acids in cell culture (SILAC; Ong et al., 2002), followed by ILK-FLAG immunoprecipitation and mass spectrometry. Among proteins with high light-to-heavy isotope ratios, indicative of specific

(I) Dynamics of peripheral caveolin (green) and MTs (red) analyzed in ILK-K5 keratinocytes treated with taxol (3 nM). Images are snapshots from Movie S3 acquired at 2 s/frame. Right panels show an enlargement of the area indicated by the white rectangle. Arrowheads indicate vesicles moving on MTs, whereas arrows indicate stabilized caveolae. Scale bar, 10 μm.

(J) Kymographs from control cells and untreated, nocodazole/taxol-treated, and taxol-treated ILK-K5 cells. Scale bars, 10 s (y axis), 1 μm (x axis).

(K) Quantification of plasma membrane (pm) caveolae of untreated and taxol-treated ILK-K5 cells (mean ± SEM; n = 41 cells (untreated)/54 cells (taxol treated) from 2 animals; ***$p < 0.0001$).

See also Movies S1–S3 and Figure S3.

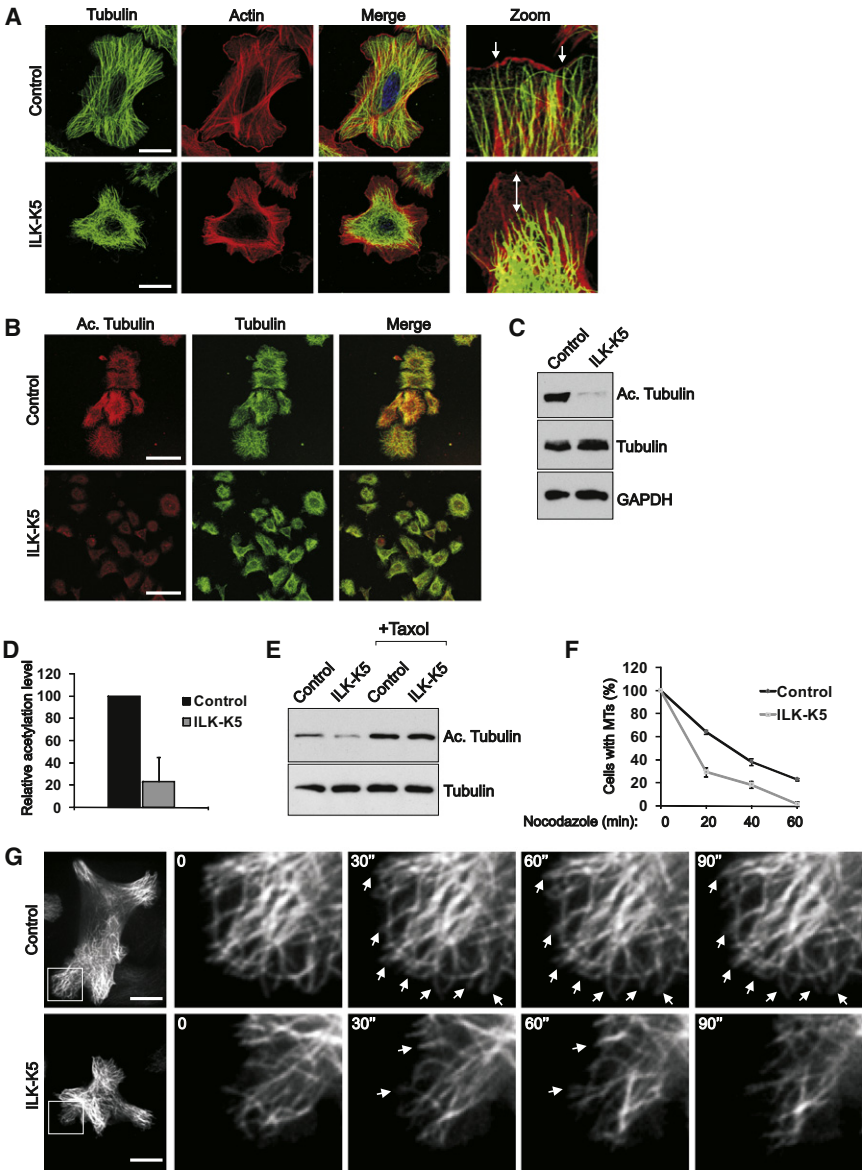

Figure 4. ILK Regulates Organization and Stability of the MT Network

(A) Control and ILK-K5 keratinocytes stained for tubulin and F-actin. Note disorganized MT network and lack of MT tip association with cortical actin (arrow) in ILK-K5 cells. Scale bars, 10 μm.

(B) Control and ILK-K5 keratinocytes stained for acetylated tubulin and α tubulin. Scale bars, 50 μm.

(C) Reduced tubulin acetylation confirmed by western blotting.

(D) Quantification of acetylated tubulin levels (average ± SD; n = 3).

(E) Control and ILK-K5 keratinocytes treated with taxol and analyzed for acetylated tubulin.

(F) Control and ILK-K5 were treated with 1 μM nocodazole for time points indicated, after which cells containing more than 10 MTs were quantified (mean ± SEM; n = 3).

(G) Dynamics of MTs analyzed by spinning-disc microscopy in control and ILK-K5 keratinocytes expressing EGFP-tubulin. Images are snapshots from Movie S4 acquired at 2 s/frame. Right panels show an enlargement of the area indicated by the white rectangle. Arrowheads indicate stable MTs. Scale bars, 10 μm.

See also Movie S4 and Table S1.

binding, were known ILK-interacting proteins, such as PINCH or parvin, as well as poorly characterized ILK-binding partners, such as IQGAP1 (Figure 6A), which has also been identified in a previous proteomic screen (Dobreva et al., 2008). IQGAP1 is an adaptor protein that localizes to the cell cortex, where it can link the MT plus ends to cortical actin by binding actin and the MT tip protein CLIP 170 (Fukata et al., 2002; Watanabe et al., 2004; Brown and Sacks, 2006). In addition, IQGAP1 can localize the activity of the formin mDia1, which can also stabilize MTs, to the cell cortex (Brandt et al., 2007).

Consistent with the proteomic data, IQGAP1 was detected by immunoprecipitation of ILK-FLAG (Figure 6B) or endogenous ILK (Figure 6C) from keratinocyte lysates. Conversely, antibodies against IQGAP1 coprecipitated ILK (Figure 6D), confirming the interaction of the endogenous proteins. In addition, mDia1 was also detected in IQGAP1 immunoprecipitates (Figure 6D). Next, we performed pulldown experiments with recombinant GST-tagged IQGAP1 in ILK-deficient fibroblasts re-expressing ILK-FLAG. These experiments confirmed the specific association of ILK with IQGAP1, and showed that deletion of IQGAP1's WW domain allowed ILK binding, while deletion of either its IQ domain or ILK's kinase domain abolished the interaction (Figure 6E). Moreover, immunostaining showed that IQGAP1 and ILK colocalized at the keratinocyte cell cortex (Figure 6F). These findings demonstrate that the interaction between ILK and IQGAP1 is specific and mediated by the kinase domain of ILK and the IQ domain of IQGAP1.

Next, we tested whether ILK regulates IQGAP1 localization. IQGAP1 was found at the cortex of control keratinocytes, where it colocalized with cortical actin (Figure 6G) and MT tips (Figure 6H). In ILK-K5 cells, the MT tips failed to extend to the cell cortex (Figure 6H), and the colocalization of IQGAP1 with cortical actin was almost completely lost (Figure 6G). Analysis of IQGAP1 localization on 20 μm-sized micropatterns confirmed that its altered localization in ILK-K5 cells was not due to reduced cell spreading (Figure S4A). Furthermore, transient re-expression of ILK-FLAG in the ILK-K5 cells rescued both IQGAP1 localization and the architecture of the MT network (Figures 6I and 6J). In addition, an IQGAP1 mutant lacking the IQ domain localized diffusely in the cytoplasm and did not colocalize with ILK, whereas a mutant lacking the C terminus, including the RasGAP, APC, CLIP 170, and mDia-binding domains, localized extensively in ILK-positive adhesions (Figure 6K). These results indicate that ILK interacts with IQGAP1, and that both ILK

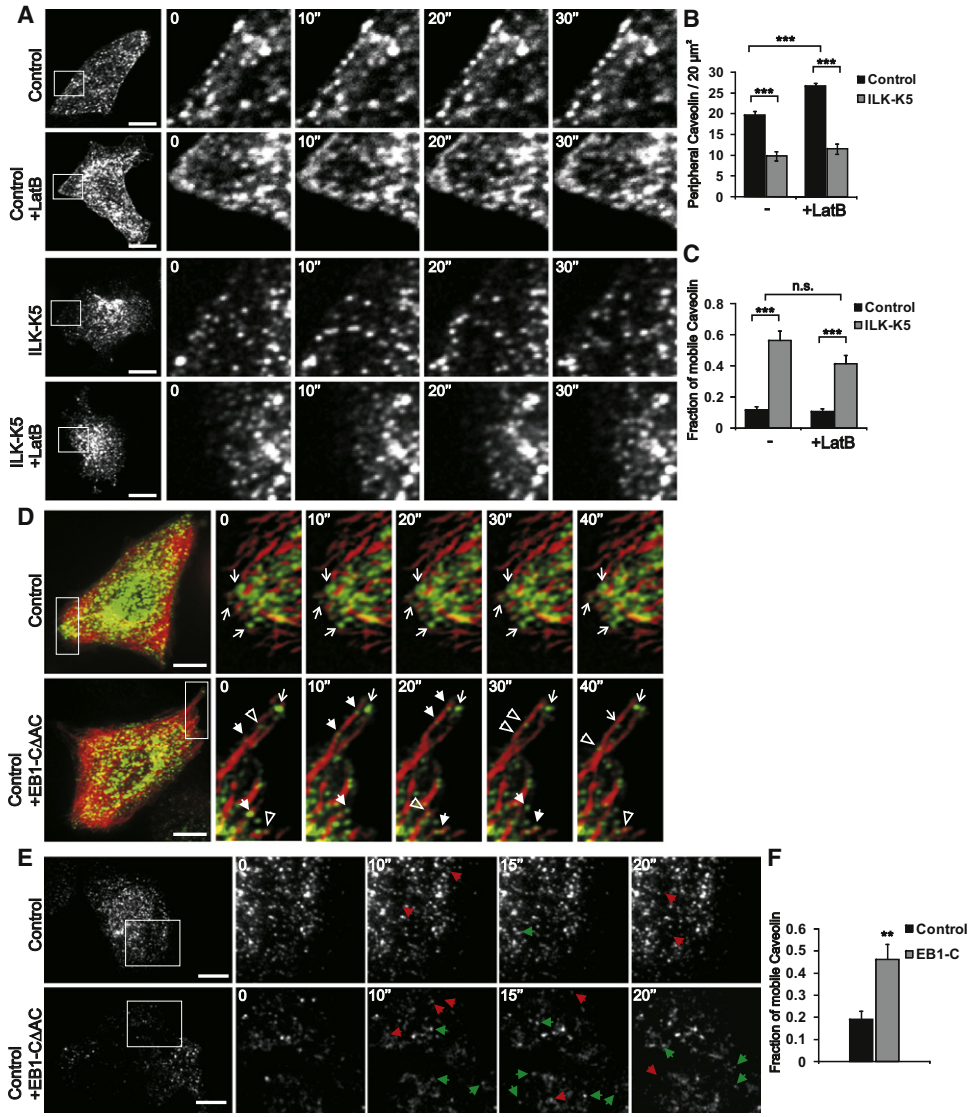

Figure 5. MT Dynamics Regulates Caveolar Trafficking

(A) Dynamics of EGFP-caveolin-1 in keratinocytes untreated or treated with LatB. Images are snapshots from movies acquired at 2 s/frame. Right panels show an enlargement of the area indicated by the white rectangle. Scale bars, 10 μm.

(B) Quantification of the peripheral density of caveolae from LatB treated cells (mean ± SEM; n = 7; ***p(ANOVA) F = 39.48; R^2 = 0.8315).

(C) Quantification of the fraction of mobile caveolin-1 from LatB-treated cells (mean ± SEM; n = 6; ***p(ANOVA) F = 23.29; R^2 = 0.7775; n.s. = not significant).

(D) Dynamics of peripheral caveolin (green) and MTs (red) analyzed by spinning disc microscopy in control cells transfected with EB1-CΔAC. Images are snapshots from Movie S5 acquired at 2 s/frame. Arrows indicate stable caveolae, whereas arrowheads and open arrows indicate vesicles moving on MTs toward the periphery or inwards, respectively. Scale bars, 10 μm.

(E) Dynamics of cell surface caveolin analyzed by TIRF in control cells transfected with EB1-CΔAC. Images are snapshots from Movie S6 acquired at ~500 ms/frame. Right panels show an enlargement of the area indicated by the white rectangle. Green and red arrowheads indicate appearing and disappearing vesicles, respectively. Scale bars, 10 μm.

(F) Quantification of the fraction of mobile caveolin-1 from EB1-CΔAC-transfected keratinocytes (mean ± SEM; n = 5; **p = 0.0079).

See also Movies S5 and S6.

expression and the IQ domain are required to localize IQGAP1 to the cell cortex.

IQGAP1 Acts in Concert with mDia1 to Regulate Caveolin-1 Trafficking

The results suggest that ILK regulates MT dynamics via IQGAP1 and possibly also mDia1. In agreement with previous reports (Watanabe et al., 2004), downregulation of IQGAP1 with siRNA resulted in decreased stability and increased dynamics of MTs in otherwise normal keratinocytes (Figures 7A–7C; Table S1B). The F-actin organization was also slightly altered in IQGAP1-depleted cells, while the localization and cell surface expression of β1 integrin, as well as the localization of ILK, were unaffected (Figures S4B and S4C and data not shown). These findings

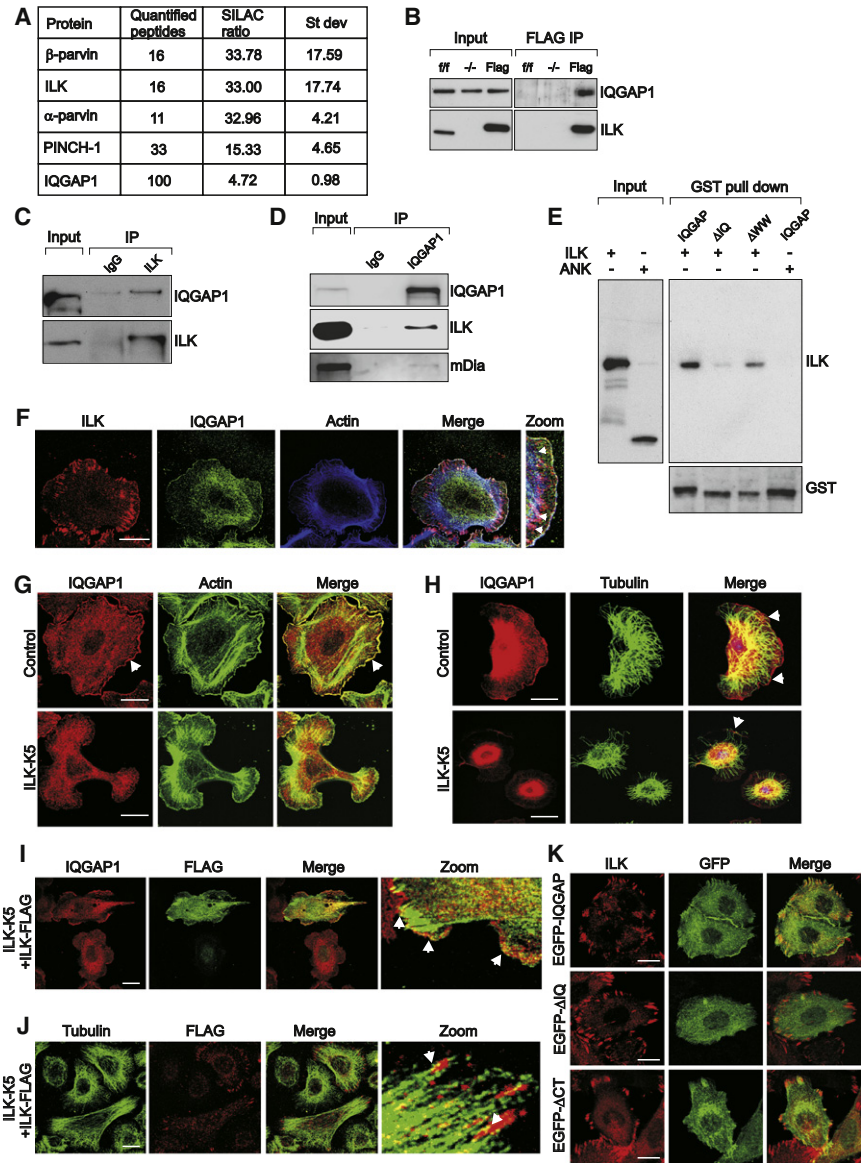

Figure 6. ILK Associates with the IQGAP1-mDia1 Complex

(A) Proteins identified from ILK-FLAG immunoprecipitates by mass spectrometry. Number of peptides and the SILAC ratio of specific to nonspecific binding are indicated.

(B) Interaction of IQGAP1 with ILK confirmed by FLAG immunoprecipitation and subsequent western blot with antibodies against IQGAP1.

(C) Interaction of endogenous ILK and IQGAP1 analyzed by immunoprecipitation of ILK.

(D) Interaction of endogenous IQGAP1 and ILK in keratinocytes analyzed by immunoprecipitation of IQGAP1.

(E) ILK pulldown from cell lysates with GST-tagged IQGAP1 or deletion mutants lacking the IQ (ΔIQ) or WW (ΔWW) domain.

(F) Keratinocytes stained for ILK, IQGAP1, and F actin. Arrowheads indicate colocalization of ILK and IQGAP with cortical actin. Scale bar, 10 μm.

(G) Keratinocytes stained for IQGAP1 and actin. Arrowhead marks IQGAP1 at the cortex of control cells. Scale bar, 10 μm.

(H) Keratinocytes stained for IQGAP1 and tubulin. MT tips align with cortical IQGAP1 in control cells (arrowheads). Scale bars, 10 μm.

(I) ILK-K5 keratinocytes transiently transfected with ILK-FLAG and stained for IQGAP1 and FLAG. Arrowheads mark cortical localization of IQGAP1. Scale bar, 10 μm.

(J) ILK-K5 keratinocytes transiently transfected with ILK-FLAG and stained for tubulin and FLAG. Arrowheads mark dense peripheral MTs. Scale bar, 10 μm.

(K) Localization of EGFP-tagged full-length IQGAP1 or deletion mutants lacking either the IQ domain (ΔIQ) or the C terminus (ΔCT). Scale bars, 10 μm.

See also Figure S4.

suggest that IQGAP1 acts downstream of ILK in regulating the MT network.

Next, we investigated the dynamics of caveolin-1 in IQGAP1-depleted cells. TIRF imaging of EGFP-caveolin showed that caveolae were static in control cells and highly dynamic in IQGAP1-depleted cells (Figures 7D and 7E; Movie S7). Furthermore, downregulation of IQGAP1 induced a relocalization of caveolin-1 from the periphery to the perinuclear region (Figure 7F). These findings resemble those of the abnormal behavior of caveolin-1 in ILK-K5 cells (Figures 1 and 3).

IQGAP1 has been shown to localize mDia1 activity to the cell cortex to regulate local actin polymerization (Brandt et al., 2007). Since mDia has also been shown to stabilize MTs (Palazzo et al., 2001), we analyzed the subcellular localization of mDia1 in ILK-K5 cells, and found its cortical localization (Figure S4D) and overall proteins levels (Figure S4E) to be reduced compared with control cells. Moreover, RNAi-resistent EGFP-IQGAP1 constructs (Figure S4F) lacking either ILK-binding (IQ domain mutant) or mDia-binding (C-terminal truncation; Brandt et al., 2007) activities failed to rescue IQGAP1 siRNA-induced defects in MT acetylation (Figure S4G).

The C terminus of IQGAP1 contains a Ras-GAP domain that has been shown to lack activity and thereby enhance Rac GTPase activity (Noritake et al., 2004; Weissbach et al., 1994). This region of the protein also serves as the CLIP-170, APC, and mDia interacting domain (Watanabe et al., 2004). We have previously analyzed Rac activity in ILK-K5 cells, and did not find it altered (Lorenz et al., 2007), pointing to mDia1 as the likely downstream target of IQGAP1 in these cells. To analyze this, we depleted mDia1 in keratinocytes with siRNA (Figure 8A). As expected, an increase in MT dynamics was observed in mDia1-depleted cells (Figure 8B; Table S1B). In addition, an increase in caveolar dynamics close to the plasma membrane was observed in these cells (Figures 8C and 8D). Furthermore,

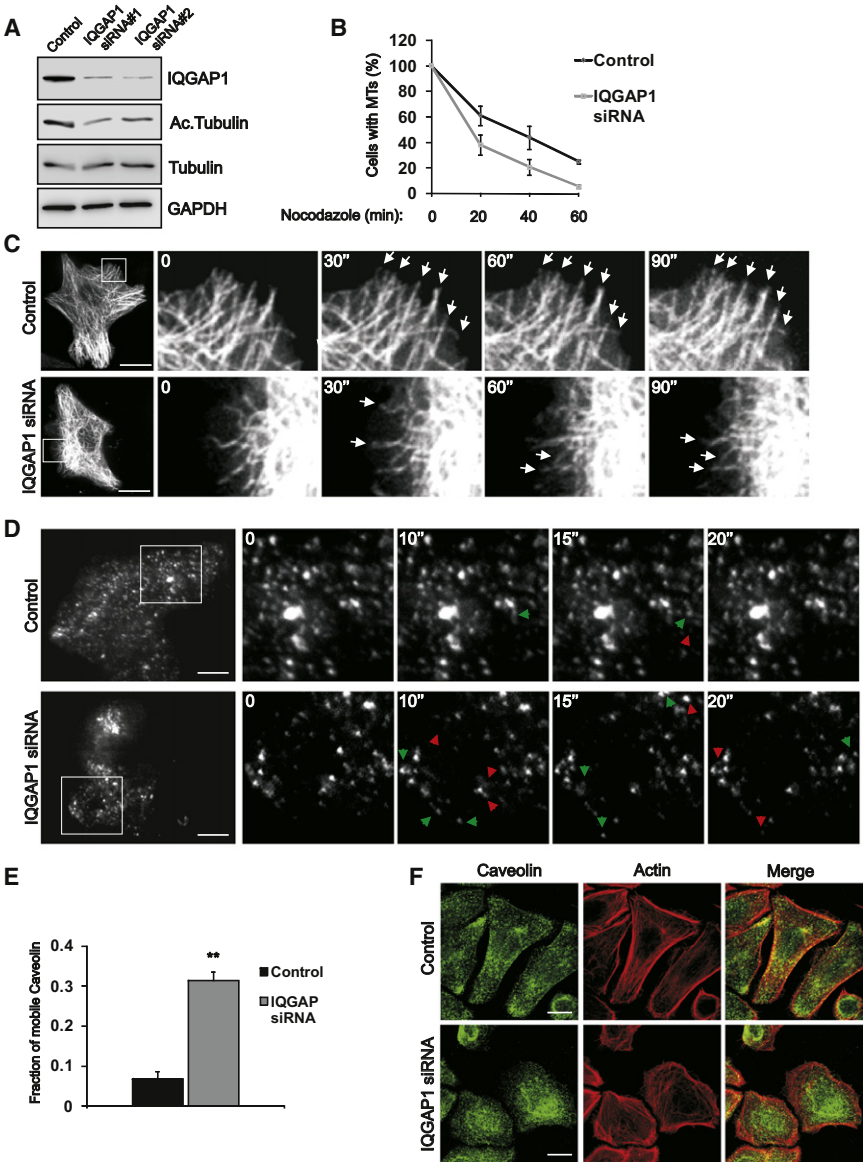

Figure 7. Depletion of IQGAP1 Destabilizes MTs and Increases Caveolin Motility

(A) Keratinocytes transfected with control or IQGAP1 siRNA and analyzed for IQGAP1 and acetylated tubulin levels.

(B) Keratinocytes transfected with control or IQGAP1 siRNA were treated with 1μM nocodazole for times indicated, after which cells containing more than 10 MTs were quantified (mean ± SEM; n = 3).

(C) MT dynamics analyzed by spinning disc microscopy in cells transfected with EGFP-tubulin and control or IQGAP1 siRNA. Images are snapshots from movies acquired at 2 s/frame. Arrowheads indicate stable MT tips. Scale bars, 10 μm.

(D) Dynamics of cell surface caveolin analyzed by TIRF in control or IQGAP1 siRNA keratinocytes expressing EGFP-caveolin-1. Images are snapshots from Movie S7 acquired at ~800 ms/frame. Green and red arrowheads indicate appearing and disappearing vesicles, respectively. Scale bars, 10 μm.

(E) Quantification of the fraction of mobile caveolin-1 from control and IQGAP1 siRNA keratinocytes (mean ± SEM; n = 5/6; **p = 0.0043).

(F) Control and IQGAP1 siRNA-transfected cells stained for caveolin-1 and actin. Scale bars, 15 μm.

See also Movie S7, Figure S4, and Table S1.

depletion of mDia1 resulted in a perinuclear localization of caveolin 1 (Figure S4H). Importantly, as in IQGAP1-depleted cells, surface expression and localization of β1 integrin were unchanged by mDia1 depletion (Figures S4B and S4C).

To further confirm that the increased caveolar dynamics in the ILK-K5 cells results from impaired MT-actin crosstalk downstream of the IQGAP1-mDia1 pathway, we overexpressed constitutively active mDia1 transiently in ILK-K5 keratinocytes. Analysis of MT dynamics revealed increased stability of peripheral MTs in the presence of active mDia1 (Figure 8E; Table S1C). Expression of constitutively active mDia1 also rescued the altered mobility of EGFP-caveolin-1 near the plasma membrane (Figures 8F and 8G; Movie S8), and resulted in the redistribution of caveolin-1, with high levels of cortical staining and colocalization with cortical F-actin (Figure 8H). These data indicate that the IQGAP1-mDia1 pathway regulates MT dynamics in keratinocytes, which is required for the trafficking of caveolin-1 to the plasma membrane.

DISCUSSION

In the present study, we show that signaling through the β1 integrin/ILK complex is required for plasma membrane caveolae formation in vivo and in vitro. In the absence of β1 integrin or ILK expression in keratinocytes, caveolae are not stably inserted into the plasma membrane due to a profound defect in MT stability. Mechanistically, ILK is required for localizing IQGAP1 to the cell cortex, which then, together with mDia1, regulates local stability of MTs. Consequently, instability of MTs is increased in cells lacking ILK, IQGAP, or mDia1, which results in increased caveolar dynamics close to the plasma membrane.

The absence of cell surface caveolae and decreased plasma membrane caveolin-1 in our EM preparations, together with increased long-range motility of caveolin-1, suggests that the β1 integrin/ILK signaling complex promotes the shuttling of caveolae between the cytoplasm and the plasma membrane. Since internalization of Ctx is not increased despite increased bidirectional trafficking of caveolae, we conclude that ILK regulates their exocytosis rather than their endocytosis. There is a strong correlation between the expression level of caveolin-1 and the presence of plasma membrane caveolae, indicating that exocytosis of caveolin-1 dictates the formation of peripheral caveolae (Parton et al., 2006). Interestingly, caveolae are maintained as stable structures throughout cycles of endo- and exocytosis, during which they are internalized and shuttled through

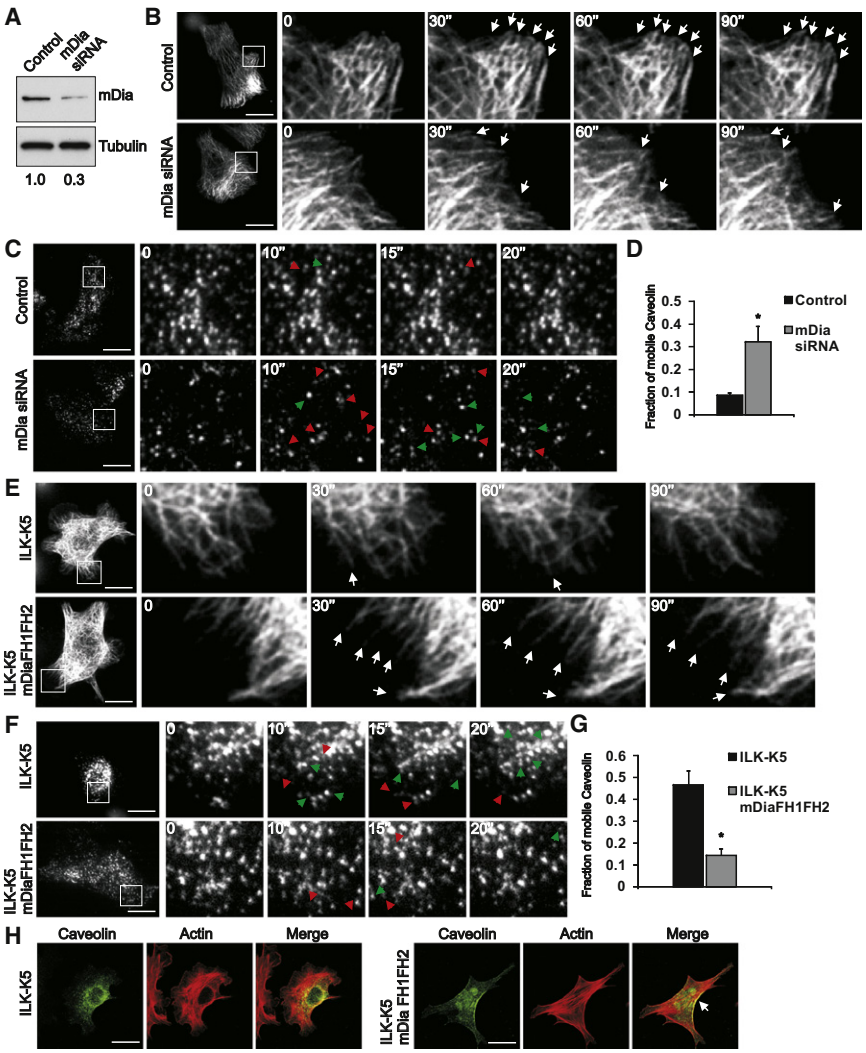

Figure 8. mDia1 Regulates MT Stability and Caveolin-1 Insertion into the Plasma Membrane

(A) Keratinocytes transfected with control or mDia1 siRNA and analyzed for mDia1 protein levels.

(B) MT dynamics analyzed by spinning disc microscopy in cells transfected with EGFP-tubulin and control or mDia1 siRNA. Images are snapshots from moves acquired at 2 s/frame. Arrowheads indicate stable MT tips. Scale bars, 10 μm.

(C) Dynamics of cell surface caveolin analyzed by TIRF in control or mDia1-depleted keratinocytes expressing EGFP-caveolin-1. Images are snapshots from movies acquired at ~800 ms/frame. Green and red arrowheads indicate appearing and disappearing vesicles, respectively. Scale bars, 10 μm.

(D) Quantification of the fraction of mobile caveolin-1 from control and mDia1-depleted keratinocytes (mean ± SEM; n = 5; *p = 0.0159).

(E) MT dynamics analyzed by spinning disc microscopy in ILK-K5 keratinocytes transfected with constitutively active mDia1 (mDia FH1FH2) and EGFP-tubulin. Arrows indicate stable MT tips. Scale bars, 10 μm.

(F) Dynamics of cell surface caveolin analyzed by TIRF in ILK-K5 keratinocytes transfected with mDia FH1FH2 and EGFP-caveolin-1. Images are snapshots from Movie S8 acquired at ~800 ms/frame. Green and red arrowheads indicate appearing and disappearing vesicles, respectively. Scale bars, 10 μm.

(G) Quantification of the fraction of mobile caveolin-1 from ILK-K5 and mDia1 FH1FH2-expressing keratinocytes (mean ± SEM; n = 4; **p = 0.0286).

(H) ILK-K5 cells expressing mDia1 FH1FH2 stained for caveolin and F-actin. Arrow indicates peripheral caveolin-1 in mDia FH1FH2-expressing cells. Scale bars, 10 μm.

See also Movie S8, Figure S4, and Table S1.

caveosomes and endosomes back to the plasma membrane (Pelkmans et al., 2004). Since we observed both increased trafficking of caveolae, as well as accumulation of caveolin-1, in endosomal structures in our ILK-K5 keratinocytes, it remains open whether the main defect is in the initial exocytotic transport or in the recycling of caveolae from endosomes back to the plasma membrane. This question is very difficult to tackle in primary keratinocytes, as their MT density is extremely high.

Our findings confirm previous studies showing that caveolar transport between the plasma membrane and intracellular compartment occurs on MTs (Mundy et al., 2002). It is not clear, however, whether MTs are also essential for the initial exocytosis of caveolar carriers. Other exocytotic carriers move on MT tracks when they traffic from the Golgi to the plasma membrane (Toomre et al., 1999), or when they are transported to basolateral or apical compartments in polarized cells (Lafont et al., 1994). Interestingly, exocytosis of the Ctx-binding GM1 requires intact MTs and also integrin-mediated adhesion (Balasubramanian et al., 2007). In line with these findings, ILK-K5 cells display strongly reduced cell surface binding of Ctx, pointing to decreased plasma membrane levels of GM1, which strongly corroborates the link between integrin signaling, MTs, and exocytosis. Some reports have also shown that secretion can occur in the absence of MTs (Rindler et al., 1987; Salas et al., 1986). However, nocadozole-mediated disruption of MTs induces dispersion of the Golgi into cytoplasmic ministacks, and thus exocytotic carriers need to cover only short distances to the plasma membrane, making random diffusion sufficient for efficient delivery (Bloom and Goldstein, 1998). Therefore, it is very likely that all exocytotic carriers, including caveolae, utilize MT tracks for long-range transport when MTs are present in cells, and MT-based transport is required to ensure the fidelity of polarized transport. In line with this, caveolin-1 transport is not completely abolished in ILK-K5 cells, as some caveolin-1 can still be detected on the plasma membrane.

The increase in bidirectional motility of caveolae near the plasma membrane is associated with loss of MT stability in ILK-deficient cells. A similar requirement of stable MTs for peripheral targeting of caveolae was also observed in wild-type cells, in which MT stability was disrupted by expressing a dominant-negative EB1 mutant. Moreover, inhibition of MT catastrophe by taxol allowed caveolae to be released from

MTs also in the absence of ILK, identifying MT stability as an important determinant of caveolar trafficking. Local stabilization of MTs, regulated by spatial cues provided from adhesion-mediated signaling, has been shown to lead to stabilizing ganglioside-containing plasma membrane rafts in fibroblasts (Palazzo et al., 2004). On the other hand, dynamic MTs have been shown to capture melanophores and initiate their minus-end-directed transport (Lomakin et al., 2009). Why caveolar vesicles are not released from the unstable MTs is not clear. Vesicle and organelle transport along MTs is driven by two families of molecular motors, dyneins and kinesins, which mediate plus- and minus-ended transport of cargo along MTs. A single cargo can employ multiple motors, but the mechanisms that regulate cargo loading and unloading at specific cellular locations are poorly understood (Verhey and Hammond, 2009). Interestingly, secretory and endocytic cargo can use a combination of MT- and actin-based transport systems (Ross et al., 2008). Outward movement of melanosomes, for example, has been shown to be regulated by crosstalk between dynein and the actin motor myosin V, where engagement of myosin V terminates dynein-driven minus-ended motility, enabling the transfer of the vesicles to actin-based motility and subsequent dispersion (Gross et al., 2002). Thus, one could, on the one hand, envisage that caveolae use distinct motors for plus- and minus-ended transport, and that the activity of these motors is differentially regulated by the dynamic instability and/or posttranslational modification status of the MT. The local stabilization of peripheral MTs could thus allow the release of the caveolar carrier, whereas dynamic MTs would capture the caveolar cargo and initiate minus-ended transport. On the other hand, decreased interactions of unstable MTs with the actin cortex, combined with the observed defects in actin organization of ILK-K5 cells, could affect the ability of caveolae to engage the myosin motor, initiate actin-based transport, and to suppress minus-ended MT transport.

It has been shown that MTs target adhesion complexes, and that repetitive targeting of adhesions by MTs can lead to the disassembly of these structures (Kaverina et al., 1998). However, adhesions can also capture MTs and stabilize them against disassembly (Kaverina et al., 1999; Krylyshkina et al., 2003). This stabilization is known to involve MT plus-end-binding proteins, which regulate the interaction between MTs and the cell cortex (Akhmanova and Steinmetz, 2008). The precise mechanisms by which adhesions attract and stabilize MTs have not been elucidated. We now identify IQGAP1 as a binding partner for ILK that links integrins in FCs directly to the MT capture complex to stabilize the MT network. FA targeting of MT tips was reduced, but not totally absent (data not shown), so it is not clear whether this function involves direct targeting of MTs to FAs as well. Our finding that ILK and IQGAP1 colocalize only in FCs suggests that this is not the case.

In agreement with previous studies, we observed plasma membrane caveolae exclusively on the basal and basolateral membranes of basal keratinocytes in vivo. The formation of a distinct lipid microenvironment at the basolateral membrane is one important mechanism to establish cell polarity. The role of actin and actin-associated proteins, as well as MTs, in the regulation of cell polarity is also well established (Siegrist and Doe, 2007; Wodarz, 2002). Thus, it seems that the β1 integrin/ILK complex functions at the interphase of these three polarity pathways, where it integrates extrinsic, ECM-derived, as well as intrinsic, MT-, actin-, and membrane-derived, polarity cues. This is consistent with the essential role of ILK in maintaining epithelial polarity in vivo (Lorenz et al., 2007; Sakai et al., 2003). Whether this mechanism applies for all cell types, however, will await further investigation.

EXPERIMENTAL PROCEDURES

Mouse Strains

To obtain a keratinocyte-restricted deletion of the *Ilk* gene, mice expressing *Cre* under the control of the keratin 5 promoter were crossed with floxed ILK mice (Lorenz et al., 2007). Offspring were genotyped as described previously (Grashoff et al., 2003).

Cell Culture and Transfection

Primary keratinocytes were obtained and cultured as described previously (Lorenz et al., 2007). Transfections were carried out with Fugene 6 (Roche). The following expression constructs were used: EGFP-caveolin-1, mDia1 FH1FH2 (Böttcher et al., 2009), EGFP/Cherry-tubulin (from R.Y. Tsien), EB1-CΔAC (from A. Akhmanova), EGFP-IQGAP1, EGFP-ΔIQ (lacking amino acids 763–863), EGFP-ΔIQ (lacking amino acids 864–1657) (from D.B. Sacks), and RFP-Lifeact (Riedl et al., 2008). ILK-Cherry was cloned by inserting human ILK cDNA (from E. Van Obberghen-Schilling) into the pCherry-N1 vector (from R.Y. Tsien).

Biofunctionalized Micropatterned Substrates

Micropatterns were generated on PEG-coated coverslips with deep UV lithography (adapted from Azioune et al., 2009). For details, see Supplemental Experimental Procedures.

Immunofluorescence

Immunohistochemical staining from skin cryosections was carried out as described previously (Brakebusch et al., 2000). For cellular immunostaining, primary keratinocytes were fixed in 3% formaldehyde or in 100% methanol, followed by incubation with primary and secondary antibodies (see Supplemental Experimental Procedures). The fluorescent images were collected by laser scanning confocal microscopy (DMIRE2; Leica) with Leica Confocal Software version 2.5, Build 1227, with 63× or 100× oil objectives.

Drug Treatments

For nocodazole resistance assays, cells were treated with 1 μM nocodazole for 20–60 min, fixed, and stained with antibodies against α tubulin. Quantifications represent three independent experiments, where 100 cells per time point were analyzed for MT content.

For inhibition of MT catastrophe, cells were treated with 3 nM taxol for 45 min prior to EM or live cell imaging analyses. For inhibition of MT growth and catastrophe, cells were treated with a combination of 50 nM nocodazole and 1 μM taxol 45 min prior to live cell imaging. For inhibition of actin polymerization, cells were treated with 0.2 μM LatB 30 min prior to live cell imaging.

EM

Skin and primary keratinocytes were processed for resin section EM and cryosection immuno-EM, essentially as described previously (Hess et al., 2010). Basal caveolae were quantified on resin sections cut perpendicularly to the BM or culturing plane. The relative distribution of caveolin-1 immunogold label was estimated by comparing gold label within a distance of < 100 nm to the plasma membrane (classified as "peripheral") with the residual gold (considered as "intracellular"). Pre-embedding immuno-EM of primary keratinocytes was performed according to standard protocols (for details, see Supplemental Experimental Procedures).

Ctx Internalization

Cells were allowed to bind fluorescently labeled Ctx (20 μg/ml; Invitrogen) for 5 or 15 min at +37°C, fixed, and analyzed by confocal microscopy. Alternatively, cells were allowed to bind Ctx for 5 or 15 min at +37°C, after which they were washed three times with 0.5 M HOAc and 0.5 M NaCl (pH 4.1) to

remove plasma membrane-associated Ctx, and analyzed by flow cytometry (FACSCalibur; Becton Dickinson). For total binding of Ctx, cells were incubated with Ctx for 15 min at +4°C, washed, and analyzed by flow cytometry. The flow cytometry data were analyzed with FlowJo software (Tree Star). For the analyses of GM1 expression, cell extracts were plotted on nitrocellulose, which was then incubated with horseradish peroxidase-coupled Ctx (Jackson ImmunoResearch) and analyzed by chemiluminescence.

Immunoprecipitation and Western Blotting

FLAG immunoprecipitation was carried out according to the manufacturers' protocol (Sigma). For immunoprecipitation of IQGAP1 or ILK, cells were lysed in 50 mM Tris-HCl (pH 8.0), 150 mM NaCl, 1% Triton X-100, 0.05% sodium deoxycholate, and 10 mM EDTA. Lysates were incubated with IQGAP1 (Santa Cruz Biotechnology) or ILK (BD Biosciences) antibodies for 30 min on ice. Isotype-matched IgG was used as a negative control. Lysates were subsequently incubated with protein G Sepharose for 1 hr and washed repeatedly with lysis buffer. Proteins were eluted from the beads with Laemmli buffer and analyzed by western blotting. Quantification of band intensities was performed with MultiGauge software (Fujifilm).

TIRF Microscopy

TIRF images were captured with an Axiovert 200M inverted microscope (Zeiss) with a 100× oil objective and a CoolSnap HQ CCD camera (Photometrics). Acquisition was controlled by Metamorph Software (Molecular Devices). Images were collected at 37°C and processed by Gaussian low-pass or median filtering and linear contrast enhancement. Motile caveolae were quantified by subtracting consecutive frames from movies.

Spinning-Disc Microscopy

Images were captured with an Axiovert 200 (Zeiss) microscope, a CSU10 spinning-disc confocal scanhead (Yokogawa), and a Cascade II EMCCD camera (Photometrics), with a 100× oil objective. Acquisition was controlled by Metamorph. Images were collected at 37°C, 5% CO_2, and processed as described above.

Quantification of MT dynamics was performed with Metamorph by creating kymographs from individual MTs. For quantification of vesicle dynamics, the positions of individual vesicles were tracked with the Track points application of Metamorph. For each vesicle, the position of the nearest MT was simultaneously tracked. The difference angle between the motility vector of a vesicle and the directionality vector of its closest MT was then calculated (403 angles in total). Angle distribution for random isotropic motility was assumed from a uniform distribution of angles between 0° and 90°. An average of 45° ± 12.99 (SD) can be obtained from this assumption.

SILAC

SILAC labeling, followed by mass spectrometry, was performed essentially as described previously (Mann, 2006). Briefly, $ILK^{-/-}$ fibroblasts (Sakai et al., 2003) expressing ILK-FLAG were cultured in medium containing heavy lysine isotope for five cell doublings. ILK f/f cells cultured in unlabeled medium were used as a negative control. The cells were subsequently lysed, pooled, and subjected to FLAG immunoprecipitation. The immunoprecipitates were separated by SDS-PAGE, followed by in-gel trypsin digestion and reversed-phase liquid chromatography (Proxeon Biosystems) coupled online to an LTQ-Orbitrap mass spectrometer (Thermo Fisher Scientific). Data were acquired with Xcalibur software and analyzed with MaxQuant software.

GST Pulldowns

The cDNA constructs encoding for GST-IQGAP, ΔIQ, and ΔWW were a gift from Dr. D. B. Sacks. Recombinant proteins were expressed and purified from *Escherichia coli*. Recombinant protein (5 μg) was incubated with 500 μg cell lysate from ILK-FLAG or ANK-FLAG, after which proteins were precipitated with glutathione beads (Novagen) and analyzed by western blotting.

siRNA

siRNA duplexes for mDia1, IQGAP1, and scrambled control were from Sigma (for sequences, see Supplemental Experimental Procedures). siRNAs were transfected with Lipofectamine (Invitrogen), and experiments were carried out 48 hr after transfection.

Statistical Analysis

Statistical evaluation was performed with GraphPad Prism software (version 5.0; GraphPad). Statistical significance was determined by the Mann-Whitney U test, except for Figure 3B and Figure 5B, where analysis of variance in combination with a post hoc Tukey test was used, and Figure 2H, where a paired t test was used. Normal distribution was confirmed with the Kolomogorov-Smirnov test (alpha = 0.05).

SUPPLEMENTAL INFORMATION

Supplemental Information includes Supplemental Experimental Procedures, four figures, one table, and eight movies and can be found with this article online at doi:10.1016/j.devcel.2010.09.007.

ACKNOWLEDGMENTS

We thank M. Grzejszczyk, K. Gutleben, A. Flörl, and B. Witting for excellent technical assistance; Dr. A. Akhmanova (Erasmus Medical Center, the Netherlands) for constructs and helpful discussions; Drs. D.B. Sacks (Brigham and Women's Hospital), R.Y. Tsien (University of California), E. Van Obberghen-Schilling (University of Nice-Sophia Antiopolis, France), and M. Aumailley (University of Cologne, Germany) for providing reagents; M. Selbach for the initial SILAC experiment; and A. Elischer for the EGFP-caveolin construct. This work was supported by the Sigrid Juselius Foundation, the Finnish Cultural Foundation, and the Academy of Finland (to S.A.W.), the Marie Curie Fellowship for Career Development within the 7th European Community Framework Programme (to J.P.), the Austrian Science Funds (grants P19486-B12 to M.W.H. and SFB021 to R.F. and L.A.H.), and the Max Planck Society (to J.P.S. and R.F.).

Received: January 11, 2010
Revised: June 6, 2010
Accepted: August 17, 2010
Published: October 18, 2010

REFERENCES

Akhmanova, A., and Steinmetz, M.O. (2008). Tracking the ends: a dynamic protein network controls the fate of microtubule tips. Nat. Rev. Mol. Cell Biol. *9*, 309–322.

Azioune, A., Storch, M., Bornens, M., Thery, M., and Piel, M. (2009). Simple and rapid process for single cell micro-patterning. Lab Chip *9*, 1640–1642.

Balasubramanian, N., Scott, D.W., Castle, J.D., Casanova, J.E., and Schwartz, M.A. (2007). Arf6 and microtubules in adhesion-dependent trafficking of lipid rafts. Nat. Cell Biol. *9*, 1381–1391.

Bloom, G.S., and Goldstein, L.S. (1998). Cruising along microtubule highways: how membranes move through the secretory pathway. J. Cell Biol. *140*, 1277–1280.

Blummel, J., Perschmann, N., Aydin, D., Drinjakovic, J., Surrey, T., Lopez-Garcia, M., Kessler, H., and Spatz, J.P. (2007). Protein repellent properties of covalently attached PEG coatings on nanostructured SiO(2)-based interfaces. Biomaterials *28*, 4739–4747.

Böttcher, R.T., Wiesner, S., Braun, A., Wimmer, R., Berna, A., Elad, N., Medalia, O., Pfeifer, A., Aszodi, A., Costell, M., and Fässler, R. (2009). Profilin 1 is required for abscission during late cytokinesis of chondrocytes. EMBO J. *28*, 1157–1169.

Brakebusch, C., Grose, R., Quondamatteo, F., Ramirez, A., Jorcano, J.L., Pirro, A., Svensson, M., Herken, R., Sasaki, T., Timpl, R., et al. (2000). Skin and hair follicle integrity is crucially dependent on beta 1 integrin expression on keratinocytes. EMBO J. *19*, 3990–4003.

Brandt, D.T., Marion, S., Griffiths, G., Watanabe, T., Kaibuchi, K., and Grosse, R. (2007). Dia1 and IQGAP1 interact in cell migration and phagocytic cup formation. J. Cell Biol. *178*, 193–200.

Brown, M.D., and Sacks, D.B. (2006). IQGAP1 in cellular signaling: bridging the GAP. Trends Cell Biol. *16*, 242–249.

Buck, K.B., and Zheng, J.Q. (2002). Growth cone turning induced by direct local modification of microtubule dynamics. J. Neurosci. *22*, 9358–9367.

del Pozo, M.A., Balasubramanian, N., Alderson, N.B., Kiosses, W.B., Grande-Garcia, A., Anderson, R.G., and Schwartz, M.A. (2005). Phospho-caveolin-1 mediates integrin-regulated membrane domain internalization. Nat. Cell Biol. *7*, 901–908.

del Pozo, M.A., Alderson, N.B., Kiosses, W.B., Chiang, H., Anderson, R.G.W., and Schwartz, M.A. (2004). Integrins regulate Rac targeting by internalization of membrane domains. Science *303*, 839–842.

Dobreva, I., Fielding, A., Foster, L.J., and Dedhar, S. (2008). Mapping the integrin-linked kinase interactome using SILAC. J. Proteome Res. *7*, 1740–1749.

Drab, M., Verkade, P., Elger, M., Kasper, M., Lohn, M., Lauterbach, B., Menne, J., Lindschau, C., Mende, F., Luft, F.C., et al. (2001). Loss of caveolae, vascular dysfunction, and pulmonary defects in caveolin-1 gene-disrupted mice. Science *293*, 2449–2452.

Fukata, M., Watanabe, T., Noritake, J., Nakagawa, M., Yamaga, M., Kuroda, S., Matsuura, Y., Iwamatsu, A., Perez, F., and Kaibuchi, K. (2002). Rac1 and Cdc42 capture microtubules through IQGAP1 and CLIP-170. Cell *109*, 873–885.

Grashoff, C., Aszodi, A., Sakai, T., Hunziker, E.B., and Fässler, R. (2003). Integrin-linked kinase regulates chondrocyte shape and proliferation. EMBO Rep. *4*, 432–438.

Gross, S.P., Tuma, M.C., Deacon, S.W., Serpinskaya, A.S., Reilein, A.R., and Gelfand, V.I. (2002). Interactions and regulation of molecular motors in *Xenopus* melanophores. J. Cell Biol. *156*, 855–865.

Hess, M.W., Pfaller, K., Ebner, H.L., Beer, B., Hekl, D., and Seppi, T. (2010). 3D versus 2D cell culture: implications for electron microscopy. Methods Cell Biol. *96*, 649–670. 10.1016/S0091-679X(10)96027-5.

Kaverina, I., Rottner, K., and Small, J.V. (1998). Targeting, capture, and stabilization of microtubules at early focal adhesions. J. Cell Biol. *142*, 181–190.

Kaverina, I., Krylyshkina, O., and Small, J.V. (1999). Microtubule targeting of substrate contacts promotes their relaxation and dissociation. J. Cell Biol. *146*, 1033–1044.

Komarova, Y., De Groot, C.O., Grigoriev, I., Gouveia, S.M., Munteanu, E.L., Schober, J.M., Honnappa, S., Buey, R.M., Hoogenraad, C.C., Dogterom, M., et al. (2009). Mammalian end binding proteins control persistent microtubule growth. J. Cell Biol. *184*, 691–706.

Krylyshkina, O., Anderson, K.I., Kaverina, I., Upmann, I., Manstein, D.J., Small, J.V., and Toomre, D.K. (2003). Nanometer targeting of microtubules to focal adhesions. J. Cell Biol. *161*, 853–859.

Lafont, F., Burkhardt, J.K., and Simons, K. (1994). Involvement of microtubule motors in basolateral and apical transport in kidney cells. Nature *372*, 801–803.

Legate, K.R., Wickström, S.A., and Fässler, R. (2009). Genetic and cell biological analysis of integrin outside-in signaling. Genes Dev. *23*, 397–418.

Lippincott-Schwartz, J. (1998). Cytoskeletal proteins and Golgi dynamics. Curr. Opin. Cell Biol. *10*, 52–59.

Lomakin, A.J., Semenova, I., Zaliapin, I., Kraikivski, P., Nadezhdina, E., Slepchenko, B.M., Akhmanova, A., and Rodionov, V. (2009). CLIP-170-dependent capture of membrane organelles by microtubules initiates minus-end directed transport. Dev. Cell *17*, 323–333.

Lorenz, K., Grashoff, C., Torka, R., Sakai, T., Langbein, L., Bloch, W., Aumailley, M., and Fässler, R. (2007). Integrin-linked kinase is required for epidermal and hair follicle morphogenesis. J. Cell Biol. *177*, 501–513.

Mann, M. (2006). Functional and quantitative proteomics using SILAC. Nat. Rev. Mol. Cell Biol. *7*, 952–958.

Mundy, D.I., Machleidt, T., Ying, Y.S., Anderson, R.G., and Bloom, G.S. (2002). Dual control of caveolar membrane traffic by microtubules and the actin cytoskeleton. J. Cell Sci. *115*, 4327–4339.

Nakrieko, K.A., Welch, I., Dupuis, H., Bryce, D., Pajak, A., St Arnaud, R., Dedhar, S., D'Souza, S.J., and Dagnino, L. (2008). Impaired hair follicle morphogenesis and polarized keratinocyte movement upon conditional inactivation of integrin-linked kinase in the epidermis. Mol. Biol. Cell *19*, 1462–1473.

Noritake, J., Fukata, M., Sato, K., Nakagawa, M., Watanabe, T., Izumi, N., Wang, S., Fukata, Y., and Kaibuchi, K. (2004). Positive role of IQGAP1, an effector of Rac1, in actin-meshwork formation at sites of cell-cell contact. Mol. Biol. Cell *15*, 1065–1076.

Ong, S.E., Blagoev, B., Kratchmarova, I., Kristensen, D.B., Steen, H., Pandey, A., and Mann, M. (2002). Stable isotope labeling by amino acids in cell culture, SILAC, as a simple and accurate approach to expression proteomics. Mol. Cell. Proteomics *1*, 376–386.

Palazzo, A.F., Cook, T.A., Alberts, A.S., and Gundersen, G.G. (2001). mDia mediates Rho-regulated formation and orientation of stable microtubules. Nat. Cell Biol. *3*, 723–729.

Palazzo, A.F., Eng, C.H., Schlaepfer, D.D., Marcantonio, E.E., and Gundersen, G.G. (2004). Localized stabilization of microtubules by integrin- and FAK-facilitated Rho signaling. Science *303*, 836–839.

Parton, R.G., Hanzal-Bayer, M., and Hancock, J.F. (2006). Biogenesis of caveolae: a structural model for caveolin-induced domain formation. J. Cell Sci. *119*, 787–796.

Parton, R.G., and Simons, K. (2007). The multiple faces of caveolae. Nat. Rev. Mol. Cell Biol. *8*, 185–194.

Parton, R.G., Joggerst, B., and Simons, K. (1994). Regulated internalization of caveolae. J. Cell Biol. *127*, 1199–1215.

Pelkmans, L., and Zerial, M. (2005). Kinase-regulated quantal assemblies and kiss-and-run recycling of caveolae. Nature *436*, 128–133.

Pelkmans, L., Puntener, D., and Helenius, A. (2002). Local actin polymerization and dynamin recruitment in SV40-induced internalization of caveolae. Science *296*, 535–539.

Pelkmans, L., Burli, T., Zerial, M., and Helenius, A. (2004). Caveolin-stabilized membrane domains as multifunctional transport and sorting devices in endocytic membrane traffic. Cell *118*, 767–780.

Pol, A., Martin, S., Fernandez, M.A., Ingelmo-Torres, M., Ferguson, C., Enrich, C., and Parton, R.G. (2005). Cholesterol and fatty acids regulate dynamic caveolin trafficking through the Golgi complex and between the cell surface and lipid bodies. Mol. Biol. Cell *16*, 2091–2105.

Riedl, J., Crevenna, A.H., Kessenbrock, K., Yu, J.H., Neukirchen, D., Bista, M., Bradke, F., Jenne, D., Holak, T.A., Werb, Z., et al. (2008). Lifeact: a versatile marker to visualize F-actin. Nat. Methods *5*, 605–607.

Rindler, M.J., Ivanov, I.E., and Sabatini, D.D. (1987). Microtubule-acting drugs lead to the nonpolarized delivery of the influenza hemagglutinin to the cell surface of polarized Madin-Darby canine kidney cells. J. Cell Biol. *104*, 231–241.

Rodriguez, O.C., Schaefer, A.W., Mandato, C.A., Forscher, P., Bement, W.M., and Waterman-Storer, C.M. (2003). Conserved microtubule-actin interactions in cell movement and morphogenesis. Nat. Cell Biol. *5*, 599–609.

Ross, J.L., Ali, M.Y., and Warshaw, D.M. (2008). Cargo transport: molecular motors navigate a complex cytoskeleton. Curr. Opin. Cell Biol. *20*, 41–47.

Sakai, T., Li, S., Docheva, D., Grashoff, C., Sakai, K., Kostka, G., Braun, A., Pfeifer, A., Yurchenco, P.D., and Fässler, R. (2003). Integrin-linked kinase (ILK) is required for polarizing the epiblast, cell adhesion, and controlling actin accumulation. Genes Dev. *17*, 926–940.

Salas, P.J., Misek, D.E., Vega-Salas, D.E., Gundersen, D., Cereijido, M., and Rodriguez-Boulan, E. (1986). Microtubules and actin filaments are not critically involved in the biogenesis of epithelial cell surface polarity. J. Cell Biol. *102*, 1853–1867.

Siegrist, S.E., and Doe, C.Q. (2007). Microtubule-induced cortical cell polarity. Genes Dev. *21*, 483–496.

Tagawa, A., Mezzacasa, A., Hayer, A., Longatti, A., Pelkmans, L., and Helenius, A. (2005). Assembly and trafficking of caveolar domains in the cell: caveolae as stable, cargo-triggered, vesicular transporters. J. Cell Biol. *170*, 769–779.

Toomre, D., Keller, P., White, J., Olivo, J.C., and Simons, K. (1999). Dual-color visualization of trans-Golgi network to plasma membrane traffic along microtubules in living cells. J. Cell Sci. *112*, 21–33.

Verhey, K.J., and Hammond, J.W. (2009). Traffic control: regulation of kinesin motors. Nat. Rev. Mol. Cell Biol. *10*, 765–777.

Watanabe, T., Wang, S., Noritake, J., Sato, K., Fukata, M., Takefuji, M., Nakagawa, M., Izumi, N., Akiyama, T., and Kaibuchi, K. (2004). Interaction with IQGAP1 links APC to Rac1, Cdc42, and actin filaments during cell polarization and migration. Dev. Cell *7*, 871–883.

Weissbach, L., Settleman, J., Kalady, M.F., Snijders, A.J., Murthy, A.E., Yan, Y.X., and Bernards, A. (1994). Identification of a human rasGAP-related protein containing calmodulin-binding motifs. J. Biol. Chem. *269*, 20517–20521.

Wickström, S.A., Lange, A., Montanez, E., and Fässler, R. (2010). The ILK/PINCH/parvin complex: the kinase is dead, long live the pseudokinase! EMBO J. *29*, 281–291.

Wodarz, A. (2002). Establishing cell polarity in development. Nat. Cell Biol. *4*, E39–E44.

Yvon, A.M., Wadsworth, P., and Jordan, M.A. (1999). Taxol suppresses dynamics of individual microtubules in living human tumor cells. Mol. Biol. Cell *10*, 947–959.